ELSEVIER

Contents lists available at ScienceDirect

Chemosphere

journal homepage: www.elsevier.com/locate/chemosphere





Soil amended with Algal Biochar Reduces Mobility of deicing salt contaminants in the environment: An atomistic insight

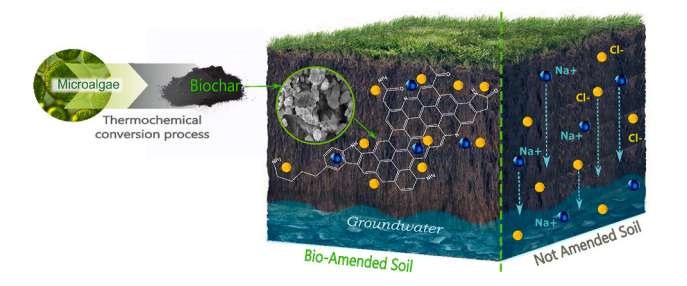
Farideh Pahlavan^a, Hamid Ghasemi^a, Hessam Yazdani^b, Elham H. Fini^{a,*}

- a School of Sustainable Engineering and the Built Environment, Ira A. Fulton Schools of Engineering, Arizona State University, 660 S. College Avenue, Tempe, AZ 85287-3005. USA
- ^b Department of Civil and Environmental Engineering, University of Missouri , W1024 Lafferre Hall, MO 65211, Columbia

HIGHLIGHTS

- Soils amended with algal biochar immobilize deicing salt contaminants.
- Type and density of functional groups on biochar affect its adsorption efficacy.
- Direct and indirect adsorption mechanisms involve electrostatic interactions.

G R A P H I C A L A B S T R A C T



ARTICLE INFO

Handling Editor: Y Yeomin Yoon

Keywords: Algae-based biochar Soil amendment Chloride adsorption Deicing salt contaminants IGMH analysis Density functional theory

ABSTRACT

Soil-based filter media in green infrastructure buffers only a minor portion of deicing salt in surface water, allowing most of that to infiltrate into groundwater, thus negatively impacting drinking water and the aquatic ecosystem. The capacity of the filter medium to adsorb and fixate sodium (Na^+) and chloride (Cl^-) ions has been shown to improve by biochar amendment. The extent of improvement, however, depends on the type and density of functional groups on the biochar surface. Here, we use density functional theory (DFT) and molecular dynamics (MD) simulations to show the merits of biochar grafted by nitrogenous functional groups to adsorb Cl^- . Our group has shown that such functional groups are abundant in biochar made from protein-rich algae feedstock. DFT is used to model algal biochar surface and its possible interactions with Cl^- through two possible mechanisms: direct adsorption and cation (Na^+)-bridging. Our DFT calculations reveal strong adsorption of Cl^- to the biochar surface through hydrogen bonding and electrostatic attractions between the ions and active sites on biochar. MD results indicate the efficacy of algal biochar in delaying chloride diffusion. This study demonstrates the potential of amending soils with algal biochar as a dual-targeting strategy to sequestrate carbon and prevent deicing salt contaminants from leaching into water bodies.

1. Introduction

Depending on terrain, human population density, and road density

and usage, tens of million metric tons of deicing salts (sodium chloride, calcium chloride, magnesium chloride) are applied to paved surfaces in cold regions worldwide annually to reduce vehicular accident rates and

https://doi.org/10.1016/j.chemosphere.2023.138172

Received 12 September 2022; Received in revised form 15 February 2023; Accepted 16 February 2023 Available online 17 February 2023 0045-6535/© 2023 Elsevier Ltd. All rights reserved.

^{*} Corresponding author.

E-mail address: efini@asu.edu (E.H. Fini).

protect the traveling public (Hintz et al., 2022). This treatment leads to heavy influxes of soluble and highly mobile ions that contaminate stormwater runoff and leach into groundwater, causing substantial aquatic salinization and toxicity and hastening the decline of trees in the roadside environment (Howard and Haynes, 1993; Marsalek, 2003; Equiza et al., 2017; Hintz et al., 2017; Jones et al., 2017; Kaushal et al., 2018; Schuler and Relyea, 2018). Deicing ions such as chloride (Cl⁻) and sodium (Na⁺) also trigger the release and transport of heavy metals such as lead (Pb) and palladium (Pt) from roadside soils and emissions of vehicle catalytic converters, further contaminating water resources and negatively affecting the environment (Amrhein et al., 1992; Bäckström et al., 2004; Paus et al., 2014; Schuler and Relyea, 2018; Aruguete et al., 2020; Saadeh et al., 2021).

Green infrastructure (GI) best management practices (BMPs) are measures that combine vegetative controls, soils, and natural processes to manage and treat contaminated stormwater before discharging it into receiving waters and aquifers (Keeley et al., 2013; Deeb et al., 2018; McFarland et al., 2019; Qiu et al., 2019; Huang et al., 2020; Mullins et al., 2020; Partenio, 2020; Xi et al., 2022). However, this infrastructure cannot permanently retain deicing salt ions, gradually releasing them into the environment (Semadeni-Davies, 2006; Stagge et al., 2012; Denich et al., 2013; Corsi et al., 2015; Robinson et al., 2017; Snodgrass et al., 2017; Burgis et al., 2020). Modification of GI as a salt mitigation strategy is needed to improve its potential to buffer surface waters from salt contaminants and reduce the groundwater salt load. A promising way to improve GI's chloride adsorption and fixation capacity is to amend the soil with biochar.

Biochar is a porous carbonaceous material derived from an animalor plant-based biomass through thermal conversion in oxygen-limited conditions (Shackley et al., 2012; Lehmann and Joseph, 2009). This process could sequester large amounts of biomass carbon in the biochar. Biochar can be used for synergistic goals such as sustainable agriculture, climate change mitigation, and contamination remediation. One of the beneficial applications of biochar is a surrogate for activated carbon in the remediation of contaminated soils (Ahmad et al., 2014; Inyang and Dickenson, 2015; Pandey et al., 2022). Amending soil with carbon-rich biochar not only improves its nutritional and biological properties and contamination resistance (Mohan et al., 2014; Olmo et al., 2016; Dai et al., 2019; Jiang et al., 2020) but could also curb the emission of greenhouse gases (GHG) like CO2, CH4, and NO2 from the soil, mitigating climate change (Cheng et al., 2008; Lehmann et al., 2008; Kuzyakov et al., 2009; Singh et al., 2012; Rajib and Fini, 2020; Rajib et al., 2021; Pandey et al., 2022). Biochar achieves these multiple targets through changing microbial activities within and physicochemical properties of the soil and creating a medium for GHG adsorption (Panahi et al., 2020). Therefore, biochar amendment is a promising way to reduce the carbon footprint of GI and turn it into a significant carbon sequestration driver (Awad et al., 2013; Purakayastha et al., 2015; Sánchez-García et al., 2019; Ghasemi et al., 2022b).

Functional groups with different characteristics (electron-donating or electron-withdrawing) might be present on the surface of biochar and its microchannels. The structural features and physicochemical properties of biochars are governed primarily by parent feedstocks and conversion process variables such as temperature and oxygen availability. For example, biochars made from biomass rich in protein (e.g., algae and sludge) contain a higher density of N-carrying groups such as pyrrole and pyridine (Leng et al., 2020). Biochars produced via fast pyrolysis have a low surface area, those produced under high-temperature conditions have high aromatic hydrocarbon content and resemble a graphitic structure (Amonette and Joseph, 2009b; Downie et al., 2009), and production in an oxygen-free environment enriches biochar with oxygenous functional groups (Fan et al., 2018; Amonette and Joseph, 2009b). High temperatures also give rise to bond-breaking in hydroxyl groups (-O-H) or other less stable functional groups in the biochar structure, resulting in more alkalinity and hydrophobicity (Li et al., 2019). Removal of acidic functional groups at high temperatures decreases the cation exchange capacity of biochar (Li et al., 2019). Like thermochemical conditions, the chemical composition and ratios of organic components of parent biomass directly impact the biochar properties. The reason lies in the fact that organic materials undergo thermal decomposition at different temperature ranges; for example, cellulose decomposes at 240–350 °C, while the appropriate temperature for lignin decomposition is in the range of 280–500 °C (Downie et al., 2009).

Structural features of biochar are a factor in determining its suitability for a specific application. For instance, more porous biochar is preferred for increasing plant productivity in hard soils, while those rich in functional groups are more effective for contamination remediation. Also, biochar's high content of organic carbon of hydrophobic nature and high surface area make it a suitable amendment for increasing the soil's water holding capacity Verheijen et al., 2010 with increases up to 18% reported in the literature (Glaser et al., 2002). The ability of biochar to adsorb organic and inorganic species through cation exchange improves soil fertility and nutrient retention. (Sohi et al., 2009), (Hajikarimi et al., 2020) In addition, the alkalinity of biochar and the abundance of organic functional groups in its highly porous structure enable it to immobilize heavy metals in contaminated soils (Zhou et al., 2020).

Since the soil in GI plays a vital role in removing and stabilizing contaminants from runoff, changes in the soil medium, specifically amending it with algal biochar, may lower the mobilization and accumulation of chloride (Cl-) ions in streams. Our prior work has shown that biochar derived from the thermochemical conversion of algae is rich in nitrogenous functional groups such as amide, amine, pyrrole, and pyridine, making it promising for selectively adsorbing some potentially hazardous bitumen emissions and retaining these volatile compounds in the matrix of bitumen (Mousavi et al., 2021). X-ray photoelectron spectroscopy (XPS), elemental analysis, and Fourier-transform infrared (FTIR) spectroscopy analysis revealed increases in the C-Cl groups at the internal surface of biochar by about 80% after HCl modification (Wang et al., 2018; Chen et al., 2022), showing the capability of biochar to adsorb chloride ions. It suggests the potential of soil amended with amine-functionalized biochar to outperform that amended with conventional biochar in adsorbing chloride from deicing salt.

The effectiveness of biochar as an economical and abundant agent for the adsorption and retention of soil contaminants largely depends on its surface area, pores volume, surface charge, and type and density of functionalities (Zhu and Pignatello, 2005). It also depends on the adsorbate's structure, charge accumulation, and interactions with active sites on biochar. Therefore, it appears imperative to optimize the production variables (biomass composition, thermochemical process, heteroatom doping techniques) to accentuate and harness favorable features of biochar for trapping deicing salt contaminants in soil and preventing them from entering groundwater. It is also essential to gain an in-depth understanding of the molecular mechanisms involved in the adsorption of Cl⁻ onto biochar. Such understanding will help produce biochar with maximum resistance to chloride diffusion.

In this study, we computationally test the hypothesis that N-containing functional groups present in algae-based biochar enhance the capacity of biochar to adsorb and retain Cl⁻. We use density functional theory (DFT) calculations and molecular dynamics (MD) simulations to illuminate the degree of reaction tendency between Cl⁻ and the functional groups of algal biochar and the underlying mechanisms involved, identifying the most effective functionals for immobilizing chloride and heavy metals.

2. Computational modeling and simulations

2.1. Density functional theory (DFT) calculations

2.1.1. Molecular structure of algal biochar

The first step to evaluating the ability of algal biochar to adsorb the

chloride ion is to construct a molecular model representative of inherently functionalized biochar derived from algal biomass. The typical approach to defining a molecular structure for individual biochar involves choices regarding the elemental composition, atomic ratios (e.g., H/C, O/C, (N + O)/C), atomic bonds in the molecule (e.g., C=C, C-C, C=O, C-H, -OH), and functional groups based on analytical and chemical analyses (e.g., Fourier-transform infrared spectroscopy, FTIR). Such characterizations have been the subject of numerous studies (Leng et al., 2015; Chen et al., 2017a, 2017b; Maliutina et al., 2018b; Chabi et al., 2020). A common denominator is that biochar is chiefly a carbonaceous skeleton decorated with surface functional groups, with the elemental composition and the type and abundance of functional groups being a function of the parent feedstock and the thermochemical process. Despite these laboratory insights, proper molecular representations of biochar remain elusive.

Based on our previously reported results for elemental information (Dandamudi et al., 2021), a decrease in the H/C atomic ratio in biochar relative to the biomass can serve as evidence for the aromatic character of algal biochar. In addition, XRD peaks at 26.426° and 43.019° (20) confirmed the presence of graphitic carbon in algal biochar that is expected to appear in the form of randomly oriented polyaromatic clusters (Dandamudi et al., 2021). Further evidence shows poorly ordered stacks of graphene layers in amorphous biochar (Keiluweit et al., 2010). So, algae-based biochar possesses a molecular structure consisting of a central amorphous aromatic zone surrounded by functional groups.

Functional groups in the biochar structure exhibit a heterogeneous composition and elicit different characteristics from the biochar surface: hydrophobic, hydrophilic, basic, or acidic. Biochar functional groups might have electron-withdrawing nature because of empty orbitals (e.g., amide or carboxylic groups) or electron-donating characteristics because of their π or σ electrons (e.g., amine or hydroxyl groups) (Amonette and Joseph, 2009b). These characteristics play a crucial role in the adsorption of organic/inorganic species (Jia et al., 2002; Zhang et al., 2017; Leng et al., 2020). As previously stated, the high-protein content of algal biomass leads to a rise in N-containing functional groups in the resulting biochar that in turn increases its adsorption capacity (Leng et al., 2020). Based on spectroscopic information, a fraction of nitrogen content in algal biomass will be retained in biochar in the form of nitrogen functionals, including amides, amines, pyrroles, and pyridines (Chen et al., 2017a; Maliutina et al., 2017, 2018b, 2018a; Chabi et al., 2020; Leng et al., 2020; Dandamudi et al., 2021). FTIR peaks also indicate the presence of oxygen-containing functional groups such as hydroxyls, phenols, carbonyl, and carboxyl in biochar. (Leng et al., 2015; Maliutina et al., 2018b; Sajjadi et al., 2019; Chabi et al., 2020; Dandamudi et al., 2021).

A schematic representation for the molecular model of algal biochar we used in the DFT computations is shown in Fig. 1. This biochar model comprises a polyaromatic graphene-like sheet surrounded by major N-and O-based functional groups. The DFT computations were intended to

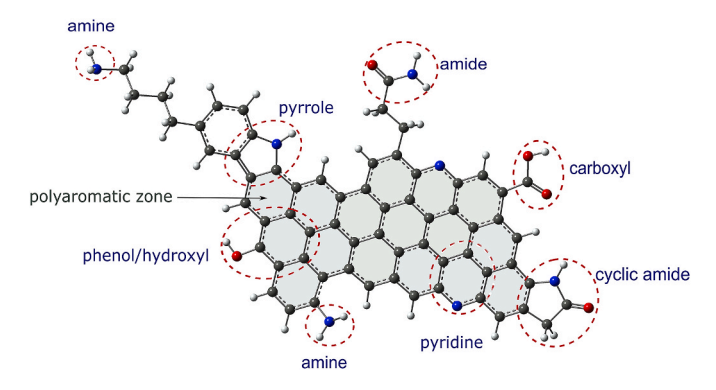


Fig. 1. Schematic of the algal biochar molecular model used in DFT computations.

elucidate the adsorption of Cl $^-$ onto the model through two potential mechanisms: 1) direct adsorption and 2) cation (Na $^+$)-bridging. The computations involved optimizing the model and all its interaction configurations with the chloride ion with the DMol3 module (Delley, 1990, 2000) (BIOVIA Materials Studio 2021). The computations were carried out using the Perdew-Burke-Ernzerhof (PBE) (Perdew et al., 1996) generalized gradient approximation (GGA) and all-electron double-numeric plus polarization (DNP) as functional and basis sets. Given the interactions expected for chloride, Grimme's long-range dispersion correction (Grimme, 2011) was included in the optimizations to accurately capture thermodynamically stable configurations and the strength of chloride adsorption on the biochar surface, PBE-D. The 'fine' level of integration was used at which the tolerances for energy, maximum force, and displacement convergence were set at 1.0×10^{-5} Hartree, 2.0×10^{-3} Hartree/Å, and 5.0×10^{-3} Å, respectively.

2.1.2. Calculation of interactions and adsorption energy

The thermodynamic stability of the chloride-biochar adsorption complexes was estimated through the adsorption/binding energy, $E_{ads}, \\$ which is the difference in energy between the adsorbed/bound state and the isolated-components state. For a two-component system consisting of the chloride ion and algal biochar, the adsorption energy between the components can be calculated as:

$$E_{ads} = E_{adsorbed} - (E_{chloride} + E_{biochar}) \tag{1}$$

where $E_{adsorbed}$ is the system's total energy in the adsorbed/bound state, and $E_{chloride}$ and $E_{biochar}$ are the energies of chloride and biochar in isolation and at thermodynamic equilibrium. A negative value for the adsorption energy of a bound system indicates a favorable gain in energy in the adsorbed state compared with the isolated state, confirming that adsorption is thermodynamically feasible. More negative values for adsorption energy are associated with stronger adsorption. (Ghasemi et al., 2022a)

The nature of intermolecular interactions is a primary factor affecting the system's stability. We used IGMH (independent gradient model [IGM] based on the Hirshfeld partitioning of molecular density) to characterize intermolecular interactions and visualize noncovalent interaction regions (Lu and Chen, 2021, 2022). IGMH is a recent adaptation of the IGM method, which was initially proposed by Lefebvre et al., 2017, 2018 based on electronic density to quantify and visualize intra- and intermolecular interactions separately through a set of 3D images that reflect the type of interactions. In comparison with other noncovalent interaction (NCI) methods, IGM achieves this practical benefit by introducing δg as a local descriptor that is defined as the difference between the gradient of promolecular density (sum of atomic densities), g, and the IGM type of density gradient (sum of absolute values of density gradient of each atom in their free states gradients), g^{IGM} (Equation (2)). Due to ignoring the sign of density gradients in the g^{IGM} definition, its value is the upper limit of g.

$$\delta g(r) = g^{IGM}(r) - g(r) \tag{2}$$

In three-dimensional cases:

$$g(r) = \left| \sum_{i} \nabla \rho_{i}^{free}(r) \right| \quad g^{IGM}(r) = \sum_{i} \left| \nabla \rho_{i}^{free}(r) \right| \tag{3}$$

where i is the number of loops over all atoms, and ρ_i^{free} denotes the spherically averaged density of the i-th atom in its free state. The IGM method can describe intermolecular (between fragments) and intramolecular (within each fragment) interactions separately as:

$$\delta g(r) = \delta g^{intra} + \delta g^{inter} \tag{4}$$

The important part of interactions for studying chloride adsorption over biochar is intermolecular interactions, defined as:

$$\delta g^{inter} = g^{IGM,inter}(r) - g^{inter}(r) \tag{5}$$

IGMH distinguishes itself from IGM by calculating the gradient of atomic density. IGMH was defined based on actual molecular electron densities instead of promolecular approximations (densities of atoms in their free states) used in the IGM method (Lefebvre et al., 2017; Lu and Chen, 2021, 2022). So, it is expected that IGMH should provide a more physically meaningful approach to exhibit interactions.

Here, we used isosurfaces of δg^{inter} to visualize interaction regions between the chloride ion and algal biochar, and meantime, to vividly reveal the nature of interactions by using different colors. The Multiwfn program (Lu and Chen, 2012) was used to perform the IGMH calculations, and the Visual Molecular Dynamics (VMD) program (Humphrey et al., 1996) was employed to export grid data to plot color-coded IGMH isosurface maps. Gaussian 16 (Frisch et al., 2016) calculations, PBEPBE/6-31G**, were used near the Dmol³ level of computations, PBE-D/DNP, to generate wavefunction files as input files required for rendering IGMH calculations in Multiwfn.

2.2. Molecular dynamics (MD) simulations

MD simulations were used to investigate the influence of the density of nitrogenous functional groups on chloride diffusion in pristine and functionalized biochar nanochannels. The biochar nanochannel model constructed for the MD simulations is shown in Fig. 2. The model consisted of a reservoir of saline water containing 1280 water molecules and seven (7) pairs of chloride (q = -1) and sodium (q = +1) ions, corresponding to 40 g/L concentration of NaCl in seawater (Lohrasebi and Rikhtehgaran, 2018). Biochar was modeled as an amorphous graphite film. The following steps were taken to construct the film (Ghasemi et al., 2022b): 1) five 5 nm-by-5nm graphene sheets were stacked at an interlayer spacing of 0.335 nm to build a crystalline graphite film, 2) in constant volume, the temperature was ramped over 50 ps from 300 K to 6000 K using the Nose-Hoover (NH) thermostat, 3) the temperature was maintained at 6000 K for 50 ps to give rise to the formation of an amorphous structure, 4) the graphite film was quenched by dropping the temperature from 6000 K to 300 K over 0.5 ps, preventing the restoration of the original crystalline configuration, and 5) the film was relaxed for 20 ps at 300 K and at constant zero pressure under the NH thermostat to obtain the final amorphous structure (Fig. 3). A time step of 1 fs was used in these steps, and the reactive force-field (ReaxFF) potential (Van Duin et al., 2001) was employed to define interatomic interactions. The graphene walls were incorporated into the model to shepherd the reservoir contents into the nanochannel. Nonadecanamide (C₁₉H₃₉NO) was used to represent amide functional groups in algal biochar (Ghasemi et al., 2022b). Its interactions were described using the Consistent Valence Forcefield (CVFF). Lennard-Jones potential was used to describe intermolecular interactions among nonbonded constituents (Table 1). Nonadecanamide was simulated at three different weight concentrations of $w_w = 0$, $w_w = 1.2\%$, $w_w = 10\%$. The thickness of the

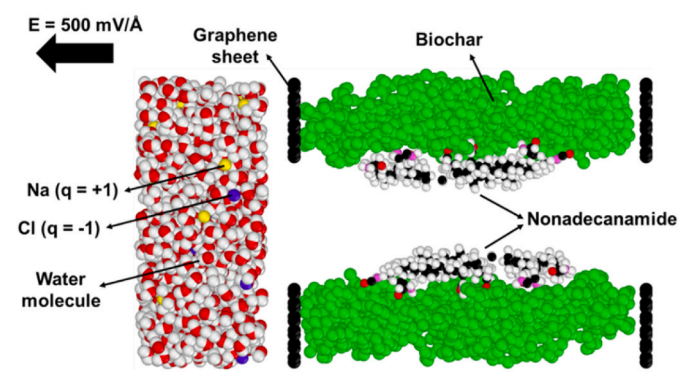


Fig. 2. The nanochannel model used for chloride diffusion.

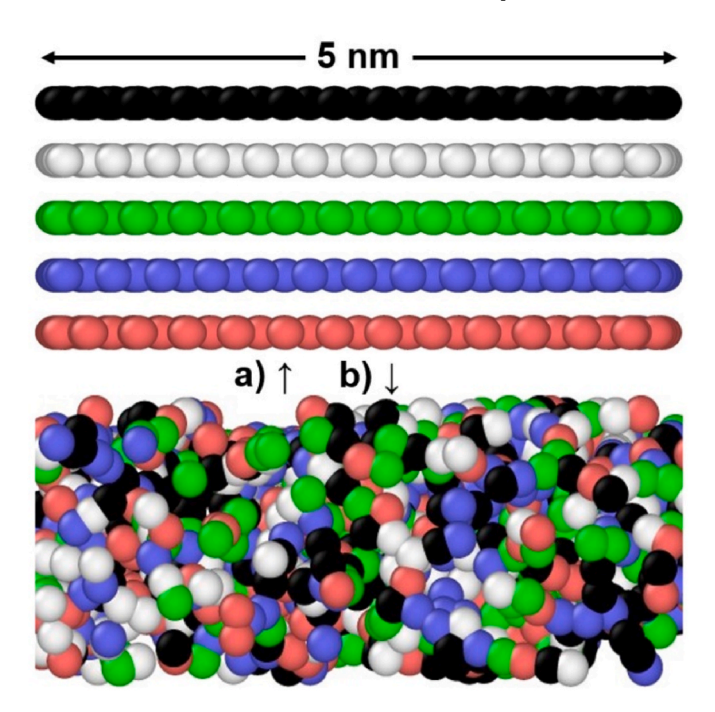


Fig. 3. Snapshots of a) Initial and b) final configurations of biochar film (graphite).

 Table 1

 Lennard-Jones coefficients of nonbonded interactions.

| atom/ion | ε (kcal/mol) | σ (Å) |
|-------------------------------------|--------------|-------|
| C in biochar | 0.069 | 3.805 |
| C (sp ³ carbon) in amide | 0.039 | 3.875 |
| C (sp ² carbon) in amide | 0.148 | 3.617 |
| H (bonded to carbon) in amide | 0.038 | 2.450 |
| H (bonded to nitrogen) in amide | 0 | 0 |
| Na | 0.003 | 3.333 |
| Cl | 0.118 | 4.420 |

opening of the nanochannel was set at 8.1 Å, three times the diameter of a water molecule (2.7 Å); for $w_w = 0$, the opening between the opposite biochar surfaces was 8.1 Å thick, and for 1.2% and 10%, it was 18.0 Å to accommodate the functional groups. All MD simulations were performed with LAMMPS (Thompson et al., 2022). A 500-mV/Å electric field was applied to all atoms in the simulation box to actuate a flow of chloride and sodium ions from the reservoir into the nanochannel and avoid reverse flow. The electric field did not have any influence on electrically neutral molecules (water, nonadecanamide, and biochar). Periodic boundary conditions were applied in all directions of the simulation box. The 'production' stage involved allowing the contents of the reservoir to flow under the dynamics applied. We continued this stage for 500 ps using a time step of 1 fs (i.e., 500,000 steps) while keeping a tally of the number of chloride ions passing the right boundary of the simulation box. This number was used to compare the efficacy of the functional group in delaying the diffusion of chloride.

3. Results and discussion

3.1. DFT-based molecular modeling

3.1.1. Electrostatic potential (ESP) colored molecular van der waals (vdW) surface for algae-based biochar

We performed a quantitative analysis of the electrostatic potential (ESP) on the van der Waals (vdW) surface of biochar to characterize the adsorption of the chloride ion—the vdW surface of a molecule is the outer hull of intersecting spheres representing atoms, with its boundary

defined by vdW radii—ESP analysis is a prevalent real space function for studying electrostatic-dominated noncovalent interactions (Politzer et al., 2001; Hunter, 2004). A visual inspection of ESP-colored molecular vdW surface maps can be used to quickly identify potential electrostatic interaction sites and qualitatively study interaction strengths. The ESP extrema (maxima [largest positive values] and minima [largest negative values]) on the molecule surface point to potential sites for nucleophilic and electrophilic attacks. The value of these ESP extrema on the vdW surface strongly correlates with electrostatic adsorption energies.

The ESP map shown in Fig. 4a depicts charge distribution over the biochar molecule. It can be seen that the surface maxima manifest on functional groups, the molecular edges, and the polyaromatic core of algal biochar due to the electron deficiency induced by the higher electronegativity of heteroatoms in substituents than that in carbon and hydrogen. The cyan dots in Fig. 4b correspond to the location of ESP maxima on the molecular surface map and denote favorable sites for chloride adsorption because the ion's negative charge makes it most attractive to ESP-positive regions.

The polarization observed in Fig. 4 can be attributed to the polar Nand O-carrying functional groups on biochar. A juxtaposition of Figs. 1 and 4 reveals the concentration of the electron-rich, blue regions around the electron-withdrawing heteroatoms of the amine, amide, pyridine, and carboxylic functional groups. These regions are unlikely to adsorb Cl-. In contrast, the adjacent electron-donating heteroatoms (-NH and -NH2 in amide, -OH in carboxylic and phenol, and -H in amines and pyrrole) colored in shades of red in the ESP map would be susceptible to chloride attack. These functionals also induce electron depletion at molecular edges. Therefore, the -CHs on the model's periphery can serve as adsorption sites for chloride. Functional groups located at the model's edges also decrease electron accumulation and increase the electrostatic potential of the polyaromatic core, which could favor chloride adsorption through π interactions with the aromatic core. The ESP maxima are located in these regions, which could be attributed to the depletion of weakly bound π -electrons from the aromatics by the Oand N-containing functional groups. Although the polyaromatic core has a higher electrostatic potential than the aromatic rings without functionalities, the Cl⁻ adsorption capacity of the aromatic part was inferior to that of polar functional groups. O- and N-carrying functional groups have higher electrostatic values (red regions) than polyaromatic zone (less intense blue). Regions covered by red-filled isosurfaces suggest that functional groups in biochar molecules increase chloride adsorption in soil.

To characterize the noncovalent interactions between chloride and algal biochar, we use the terms $\pi\text{-hole}$ and $\sigma\text{-hole}$ referring to regions with lower electronic densities (corresponding to the positive ESP values on the vdW surface). $\pi\text{-}$ and $\sigma\text{-holes}$ can behave as electron-acceptor to form noncovalent interactions dominated by an electrostatic attraction caused by the depletion of $\pi\text{-}$ and $\sigma\text{-electrons}$ in these regions. The surface maxima located at the opposite side of an atom with respect to a covalent σ bond is labeled $\sigma\text{-hole}$, which can potentially extend that bond with approximately linear interactions (Clark et al., 2007). The surface maxima located perpendicular to the molecular plane are known

as a π -hole (Politzer et al., 2010; Hennemann et al., 2012). An electrostatic extrema analysis on the vdW surface of the molecule can reveal the π - and σ -holes, and the ESP value at extrema is directly related to the strength of the corresponding π - or σ -hole bonding. Surface maxima shown in Fig. 4b correspond to the π -holes and σ -holes, and the ESP positive region around a maximum point is a measure of π - or σ -hole size

3.1.2. Influence of functional groups on electron distribution on biochar surface

We performed electrostatic analysis and ESP map visualization for a simple graphene-like structure in pristine and functionalized forms to study the influence of functional groups on electron density distribution on the vdW surface of a polyaromatic structure. The structure studied was coronene (C₂₄H₁₂, also known as superbenzene and cyclobenzene), a polycyclic aromatic hydrocarbon comprising seven peri-fused benzene rings. Two different functional groups substituted a carbon at the edge of electron-rich coronene; amine and hydroxyl representing electrondonating groups, and amide and carboxylic typifying electronwithdrawing groups. These functional groups were expected to induce changes in the π -electronic distribution and, consequently, the ESP maps. Changes in the ESP map of polyaromatic arise from the conventional views of the nature of the substituents. Results shown in Fig. 5 indicate that electron-withdrawing groups (amide and carboxylic) slightly deplete electron density above the polyaromatic core (reduction of the π -electron density), weakening repulsion between the π -electron cloud of coronene and electron-rich species like anions. In contrast, substituents with electron-donating characteristics (hydroxyl and amine) increase electron density (darker shades of blue) above the polyaromatic core, resulting in more negative ESPs.

As discussed later, changes induced by functional groups in the π -electron density of the aromatic core are not important. Light-blue areas of the ESP isosurface over aromatic rings in the functionalized coronene imply weak, if any, chloride adsorption over the π -system of the polyaromatic core. However, substitution further enhanced the ability of the polyaromatic core to bind the anion because of the induced electron depletion on the polyaromatic core and less steric effects. Interaction configurations of Cl $^-$ with algal biochar presented in the next section corroborate the insignificance of the induced changes in the aryl π -electron density. Despite the minor changes in electron density over the polyaromatic core, functionalization enhanced the affinity of graphene-like structure representing algal biochar for the chloride anion. Notably, the ESP maps show significant electron density depletion at functional groups (isosurfaces of darker shades of red) corresponding to active sites of stronger attractive interactions with Cl $^-$.

3.1.3. Mechanism of chloride adsorption over the algal biochar

3.1.3.1. Direct adsorption. The structural and energetic landscape of potential interactions between Cl⁻ and algal biochar were investigated using DFT-based computations to gain insight into noncovalent interactions involving functional groups and the polyaromatic core of

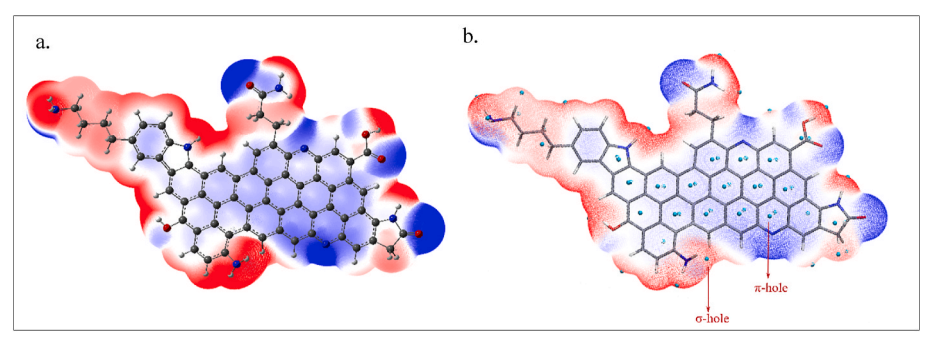


Fig. 4. a) ESP-colored molecular surface map on a BWR (blue-white-red) scale; the red- and blue-filled surfaces correspond to electron-depleted and electron-accumulated regions, respectively. Values range from -22~kcal/mol (blue) to 22~kcal/mol (red). b) surface extrema dots with cyan color on ESP and examples for π - and σ -holes. Note: in b), the ESP surface has been transparentized to make ESP extrema on the backside visible. (For interpretation of the references to color in this figure legend, the reader is referred to the Web version of this article.)

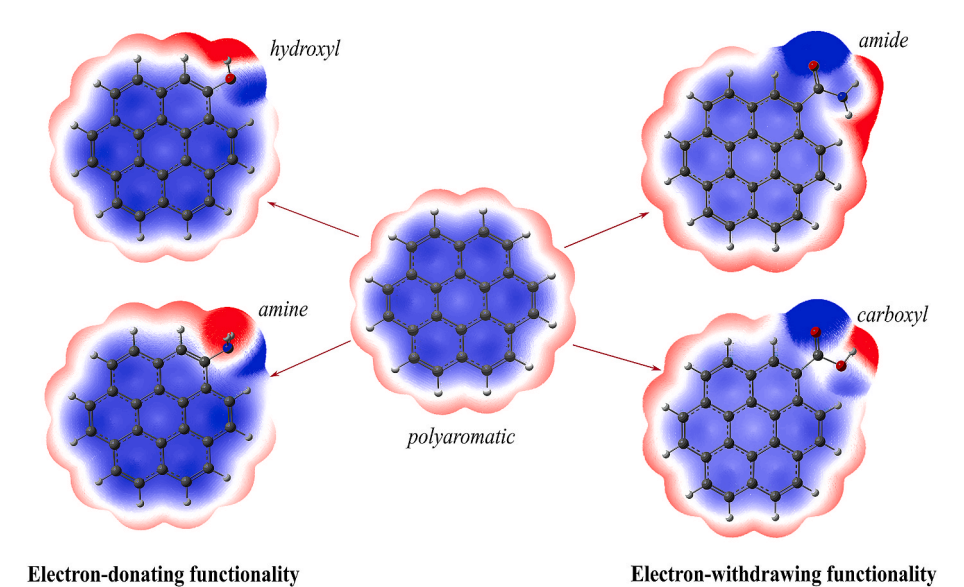


Fig. 5. ESP maps on electron density isosurfaces for coronene with and without functional groups. The red color corresponds to regions with low electron density (positive ESP), and the blue color indicates regions with high electron density (negative ESP). (For interpretation of the references to color in this figure legend, the reader is referred to the Web version of this article.)

algal biochar and develop a conceptual foundation for the feasibility of using algal biochar to adsorb deicing ions such as Cl⁻ in soil. Adsorption of a target ion on algal biochar is a thermodynamic process governed by the difference between stability energies in isolated and complex forms (Equation (1)). This difference determines the strength of ion adsorption and the capacity of algal biochar to restrain deicing contaminants in soil.

As previously stated, ESP maxima (electron-deficient regions) are the most probable active sites for chloride adsorption. The adsorption energies and IGMH maps for ${\rm Cl}^-$ adsorption on these sites are shown in

Fig. 6. The figure was constructed after a thorough search over the entire biochar structure for all possible adsorption configurations with Cl^- , given that active sites for chloride adsorption are not limited to specific functional groups, and their reactivity could be overshadowed by substituents and aromatic rings coordinated to the functional groups. This is of particular importance because the electron-withdrawing or electron-donating characteristics of substituents near the functional group could considerably affect the interactions of functional groups with the chloride ion, as evidenced by the b and f configurations in Fig. 6, where the

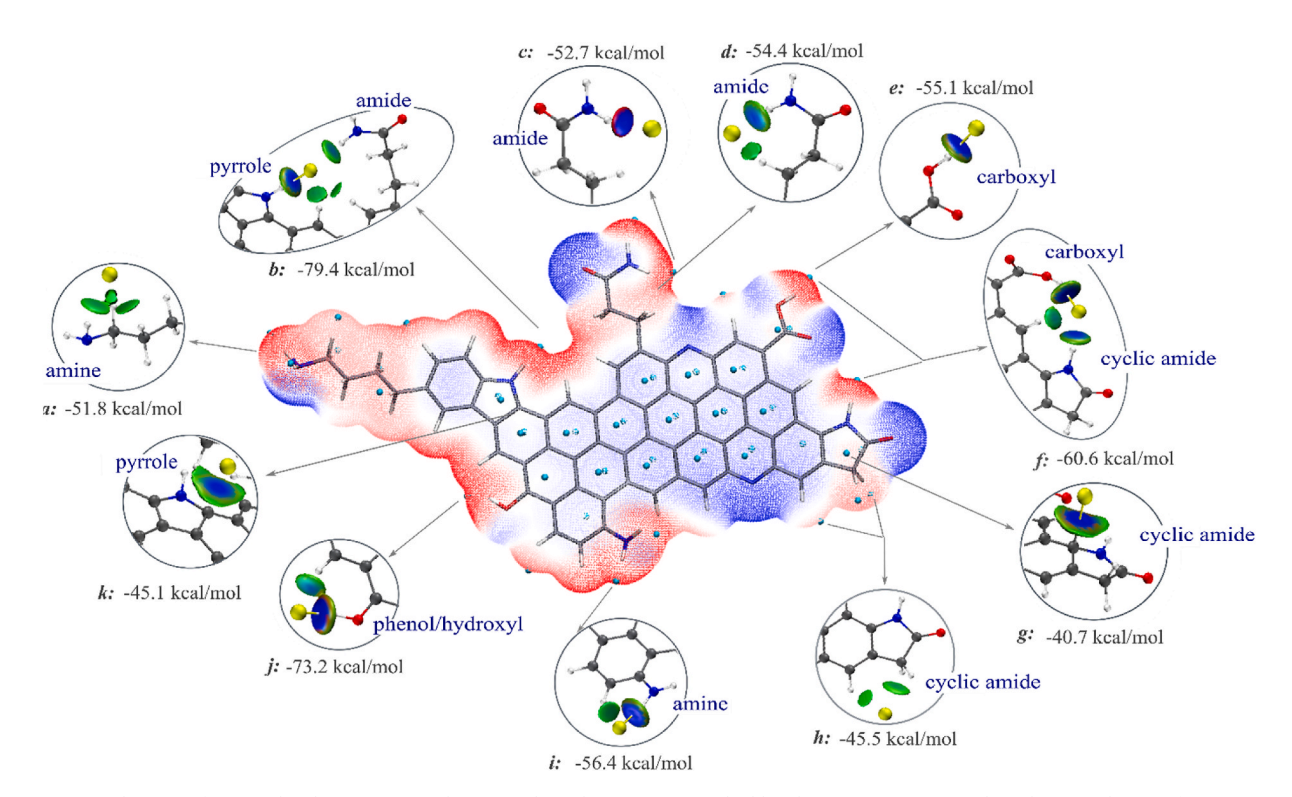


Fig. 6. IGMH visualization of intermolecular interactions between Cl⁻ and active sites on algal biochar. Active sites are selected among dozens of ESP maxima (cyan dots) on the electrostatic potential surface of the biochar molecule. The carbon, hydrogen, nitrogen, and oxygen atoms and the chlorine ion are colored in gray, white, blue, red, and yellow, respectively. The IGMH map is on a BGR (blue-green-red) color scale: blue for attractive (like H-bonding), green for vdW, and red for repulsive interactions. (For interpretation of the references to color in this figure legend, the reader is referred to the Web version of this article.)

chloride ion has found its stable equilibrium location between two functional groups.

3.1.4. Ionic hydrogen bonding

The DFT computations showed that chloride anions preferentially sit on the molecular plane of the polyaromatic algal biochar coordinating via electrostatic interactions and hydrogen bonds to C-H and functional groups located at the biochar edge (σ-hole bonding). The E_{ads} negative values for all chloride-biochar interacting configurations reported in Fig. 6 corroborate that Cl⁻ adsorption onto algal biochar is thermodynamically feasible. The extent of adsorption strength (i.e., Eads values), however, depended on the functional group. For example, the chloride ion shows the maximum adsorption to the pyrrole and phenol sites in the σ -hole bonded configurations b and j, with E_{ads} values of -79.4 and -73.2 kcal/mol, respectively. In contrast, Cl⁻ was found to have the weakest interaction with cyclic amide ($E_{ads} = -40.7 \text{ kcal/mol}$) and pyrrole ($E_{ads} = -45.1 \text{ kcal/mol}$) to form $\pi\text{-hole}$ bonded complexes. The difference observed in the affinity of Cl⁻ for different functional groups is due to the distinct intermolecular noncovalent interactions involved, as discussed below.

The IGMH colored maps (Fig. 6) show the main interaction regions between the guest Cl⁻ and the host biochar for all adsorption configurations a to k. Based on energy results and IGMH visualizations shown in this figure, the best performance of algae biochar is related to its Cl⁻ adsorption through "ionic hydrogen bonding" interactions (Meot-Ner, 2012; Ashworth et al., 2016). Fourier-transform infrared spectroscopy (FTIR) analysis and bond-energy measurements based on the adsorption isotherm data reported in the literature also showed that hydrogen bonding occurred between chloride and the electropositive H atom in polar functional groups at the surface of activated carbon is the major mechanism for chloride adsorption (Sun et al., 2017). Because of the similarity of biochar's structural and element composition to that of activated carbon, biochar has similar molecular and interacting behavior and performance.

In each adsorption configuration shown in Fig. 6, the Cl⁻ ion forms a hydrogen bond with the O-H or N-H segment of a functional group and the adjacent C-H bond, resulting in a thermodynamic stabilization for chloride over algal biochar. Here, ionic hydrogen bonding is represented by $X-H...Cl^-$ (X = O or N), where hydrogen intercedes between two heteroatoms with high electronegativity. The strength of ionic hydrogen bonds is proportional to the negative charge on the anion (here, chloride). The observed ionic H-bonding interactions between the biochar and chloride are in the reasonable short H...Cl⁻ distances and X-H...Cl⁻ angles close to 180° , similar to the ordinary H-bonding. From the IGHM maps, it is found that the δg^{inter} isosurfaces with the blue-colored center mainly occur in regions between chloride and hydrogen atoms attached to the N- or O-carrying functional groups; Cl - ... H-N, Cl - ... H-O, and Cl⁻ ... H–C. Among these interactions, the first two are stronger than the last one because of the higher electron density accumulated in their interacting regions (shown in dark blue in the central area of elliptic isosurfaces in Cl- ... H-N and Cl- ... H-O ionic hydrogen bonds). However, depending on the nature of the functional group and its position in the biochar molecular structure, ionic H-bondings in Cl- ... H-N or Cl - ... H-O have different strengths, as confirmed by the five different blue color intensities exhibited for the Cl^- ... $\mathrm{H} ext{-}\mathrm{N}$ interaction in *a*, *b*, *c*, *d*, and *f* complexes. IGMH for Cl⁻ ... H–N in the *a* configuration reveals a distinctly green color, indicating that this interaction is weak, though not negligible. The $\mathrm{Cl}^- \dots \mathrm{H\!-\!C}$ interactions in all reported configurations in Fig. 6 are revealed by the green color of the IGMH isosurfaces, indicating a lower electron density in their interacting regions than for Cl⁻ ... H–N and Cl⁻ ... H–O and suggesting the interaction was fully dispersion-dominated. There might be a stronger dispersion interaction between Cl⁻ and C-H in the high electron deficient areas (darker shades of red in the ESP). In configuration i, Cl⁻ ... H-C is unveiled by the light blue region in the center of the green IGMH isosurface, indicating a higher electron density in the interaction region and

stronger binding than the other common Cl⁻ ... H–C interactions.

3.1.5. Anion- π interactions

The polyaromatic core is regarded as a source of π -electron density, and based on chemical intuition, it is expected to interact with chloride anions repulsively. However, substitutions can alter the electron distribution in the π -system and change the strength of forces between the anion and the aromatic ring. Interesting findings confirm the existence of attractive noncovalent interactions between anions and the electrondeficient π -system of aromatic rings, referred to as "anion- π interactions" (Quiñonero et al., 2002, 2004; Schottel et al., 2008; Giese et al., 2011, 2016), where the anion acts as electron donor, and the π -system serves as electron acceptor. The interactions of an anion situated atop a substituted aromatic ring is not due to its attraction toward the π -system. Instead, it is because of favorable interactions of the anion with the substitutions or atoms carrying positive potential in the vicinity of substitutions that overwhelm the unfavorable repulsion between the anion and the aromatic ring (Wheeler and Bloom, 2014). Although the electron density over the polyaromatic core of biochar decreases because of the electron-withdrawing characteristics of some functional groups, the interaction of Cl⁻ with the π -system of polyaromatic is unfavorable. This behavior is due to π -electron accumulation, though in lower density (light-blue ESP) than the virgin polyaromatic, repelling the chloride ion. In some configurations, favorable interactions of Clwith the functional groups overwhelm its unfavorable repulsion against the aromatic ring of algal biochar. In initial configurations designed for the chloride- π interacting complexes, dispersion forces push chloride to a position over functional groups, concomitant with the formation of ionic H-bonding with a functional group, Cl⁻ ... H–N or Cl⁻ ... H–O. The d and b configurations resulted from these switching reaction mechanisms. However, in some adsorption configurations (k and g), Cl⁻ ions moved to above the aromatic plane because of the electron deficiency of the π -system favoring π -hole bonding.

Our DFT-based computations demonstrate that somewhat anion- π interactions dominated by electrostatic effects occurred in the energetically favorable chloride-biochar adsorption complex (-45.1 and -40.7 kcal/mol for k and g configurations, respectively). These results suggest that N-substitution in the biochar molecular structure (pyrrole and cyclic amide) caused a concentration of positive potential on the neighboring carbons and created active sites to adsorbed chloride anion in the vertical direction with respect to the polyaromatic plane, π -hole bonding. The blue spot at the center of the surface region in the IGMH maps of the k and g adsorptions unveil notable attractions between Cl⁻ and carbons in the pyrrole or cyclic amide motif. The Cl⁻ ... C in these complexes should be strong and stable, signified by the prominent blue color. Further, the green region in the IGMH maps of k and g indicates a dispersion-dominated interaction between the chloride and rings.

3.2. Cation-bridging mechanism

3.2.1. Cation- π interaction

Among functional groups, those with the ability to pair with cations, including Na $^+$ or proton (H $^+$), can serve as hooks to hold Cl $^-$ ions in the soil and prevent their transport. The concentration of electrons in the negative potential surface of ESP over functional groups (blue-colored ESP surface in Fig. 4) can induce strong attraction to Na $^+$ and improve the electrochemical Na $^+$ storage and, subsequently, Cl $^-$ storage capacity through the cation-bridging mechanism. As shown in Fig. 4, the amide, carboxylic, and pyridine electron-withdrawing groups carry a negative potential needed to adsorb the sodium cation. Therefore, electrostatic attractions between Na $^+$ and these functional groups are likely predominant. On the other side, the π -electrons of the polyaromatic core of the algal biochar structure may be sufficiently electron-donating to bind Na $^+$, resulting in a source of delocalized positive charge attracting the chloride ion. Cation- π interaction is a strong non-covalent interaction that is expected to contribute to the adsorption of

Na $^+$ on the polyaromatic core of algal biochar. Cation- π interaction involves the π -electron distribution of aromatic rings in which cation lies above the aromatic ring (Cubero et al., 1998). Unlike anion- π , this attraction between cation and π -electron cloud is consistent with chemical intuition. Although cation- π is generally dominated by polarization induced by cation and electrostatic forces (Cubero et al., 1998), cation- π interactions in nonpolarizable sodium cation can be explained by electrostatic considerations.

To gain a molecular-level insight into the configurations and interactions in the bridging mechanism, Na+- Cl- adsorption over four active sites of biochar was investigated. Fig. 7 shows the adsorption complexes and color-coded IGMH maps for interactions between algal biochar and the deicing salt ions, Na^+ and Cl^- . High adsorption energies for the Cl⁻·•·•Na⁺·•·•biochar complexes support this hypothesis that the noncovalent interactions of chloride anion with the Na⁺. • • • biochar provide high stability for the adsorption complex. In the Na ⁺ -bridging mechanism, functional groups with high electron concentrations and negative potential, such as pyridine, could be involved in the cation (here Na⁺) adsorption. The adsorption energies shown in Fig. 7 are deemed to be adequate to fall in the range of strong electrostatic and ionic interactions: the adsorption of Cl⁻ (I) over the Na ⁺ adsorbed on pyridine with $E_{ads} = -130 \text{ kcal/mol}$, (II) on Na⁺- carboxylic with E_{ads} =-142.3 kcal/mol, (III) on Na $^+$ -cyclic amide with $\rm E_{ads}=-119.5$ kcal/ mol, and (IV) on Na⁺-polyaromatic surface with $E_{ads} = -120.6$ kcal/ mol. Higher adsorption energies in complexes I and II are furnished by the strong attraction of Cl from the other side toward the electrondeficient functional groups carrying positive potential, i.e., amine (-NH₂) in complex I and hydroxyl (-OH) of carboxyl in complex II. The blue color on the central area of the IGMH elliptic isosurfaces in Cl - ... $\mbox{H--N}$ and \mbox{Cl}^- ... $\mbox{H--O}$ suggests strong ionic hydrogen bonds. Even without considering high energy values, the IGMH isosurfaces in Fig. 7 reveal the strength and regions of intermolecular interaction between ions and algal biochar, indicating the high stability of chloride adsorption over algal biochar. For instance, the light blue color regions on the δg^{inter} isosurface showing the interaction between Na⁺ and Cl⁻ indicates notably denser electron fields than in the green dispersion interaction

regions. The green color on the IGMH isosurface between Na $^+$ and the polyaromatic surface of biochar, complex IV, indicates the presence of electron density in this region that points to a dispersion-dominated cation- π interaction.

Soil chemistry such as pH may also affect the adsorption of deicing salt ions onto biochar. Protonation and deprotonation of surface Ocontaining functional groups (mostly hydroxyl and carboxylic acid groups, -COH and -COOH) (Mukherjee et al., 2011; Leng et al., 2015; Chabi et al., 2020) in the structure of N-rich algal biochar under acidic and alkaline could be responsible for the surface positive and negative charge of biochar, influencing the Cl- and Na+ fixation and consequently their immobilization in the soil. O-containing functional groups become negatively charged on deprotonation, which positively influences Na ⁺ fixation, and, in turn, the immobilization of Cl⁻ in soil. As previously noted, the content of O-containing functional groups in biochar depends on feedstock and pyrolysis temperature. The total amount of hydroxyl and carboxyl groups decreases with the pyrolysis temperature, resulting in a reduction in the number of deprotonatable groups and a corresponding drop in the surface negative charge and anion storing. Besides the deprotonability of -COH and -COOH, protonation of these functional groups in low pH conditions leads to positively-charged surfaces in biochar that are compensated by anions such as Cl⁻.

3.3. Molecular dynamics (MD) results

Results of the MD simulations are shown in Fig. 8. The functional group is seen to be less effective at low fractions. However, doping algal biochar with 10 wt% nonadecanamide increased its chloride uptake capacity by nearly 9.6%. No signs of an increase in chloride diffusion are observed in the individual functionalized cases, as evidenced by their linear trend. Computational power permitting, considerably longer simulations will shed light on how the accumulation of ions in the nanochannel or saturation of functional groups would influence the long-term efficacy of algal biochar in retaining chloride. Also, functional groups of varying types in contents well above 10% are expected in biochar (Dandamudi et al., 2021). Simulation of biochars heavily functionalized with various groups, which is reserved for future work,

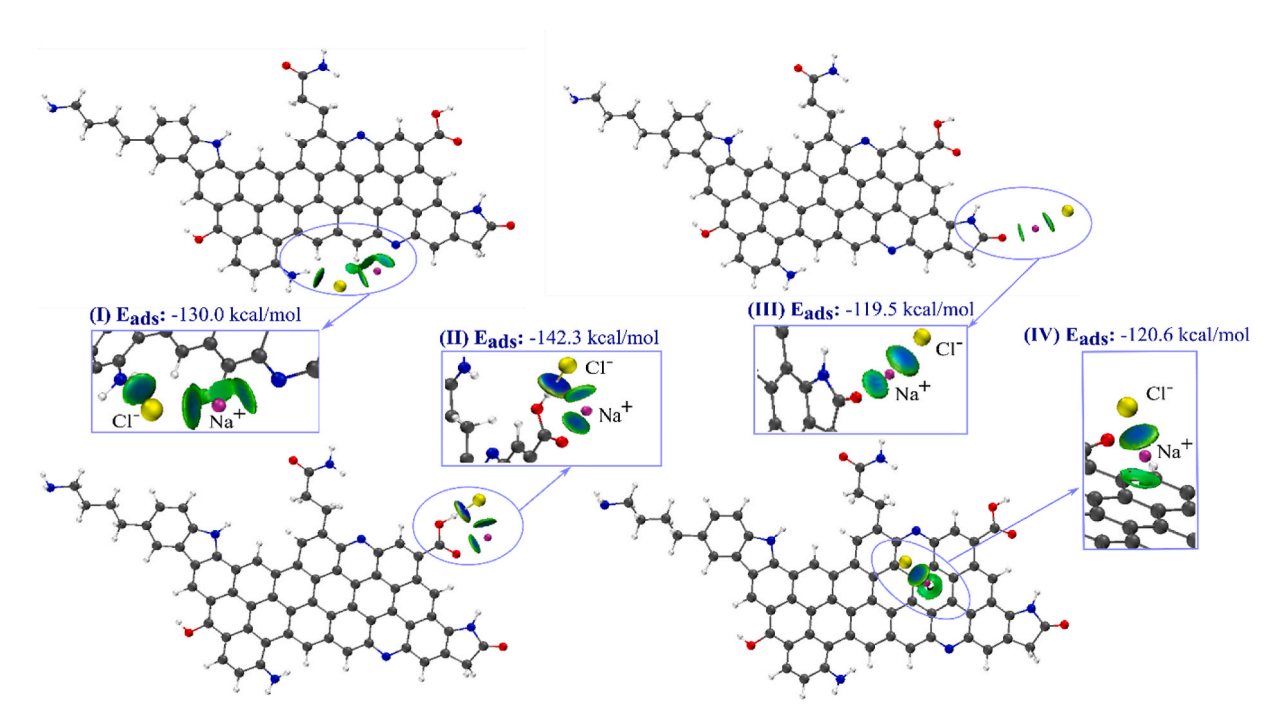


Fig. 7. Adsorption of chloride (Cl⁻) on the algal biochar through a cation (Na⁺)-bridging mechanism, and IGMH visualization of intermolecular interactions between Cl⁻ and Na⁺-algal biochar complex. Carbon, hydrogen, nitrogen, oxygen atoms, chloride, and sodium ion are shown in gray, white, blue, red, yellow, and purple, respectively. (For interpretation of the references to color in this figure legend, the reader is referred to the Web version of this article.)

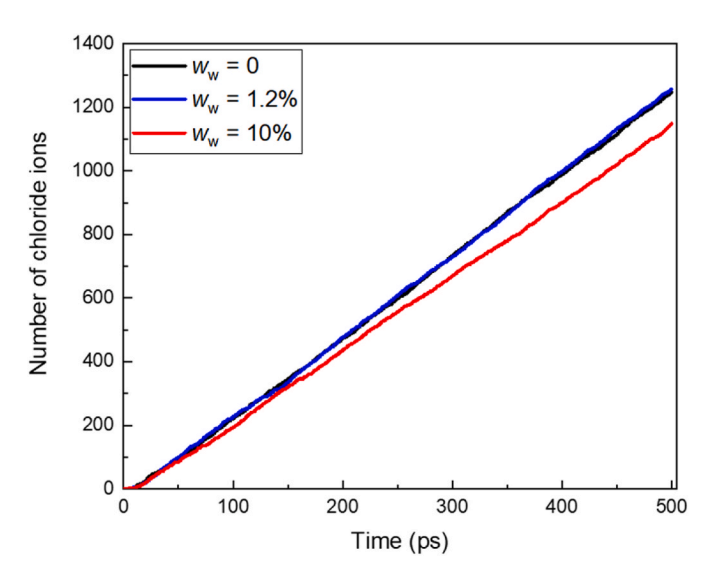


Fig. 8. History of chloride ions exiting the right end of the MD simulation box.

will help identify the corresponding combinations of feedstocks and processing conditions that would optimize the adsorption capacity of biochar.

4. Conclusion

The potential of nitrogen-rich algal biochar as an amendment to attenuate the infiltration of chloride from deicing salts into soils and the mechanisms involved were computationally studied. DFT computations were performed to illuminate interactions and mechanisms governing the immobilization of chloride by algal biochar. MD simulations were also carried out to cast light on the influence of the density of nitrogenous functional groups on chloride diffusion in pristine and functionalized biochar nanochannels. The DFT computations showed the contribution of some of the most common interactions like electrostatic, anion-/cation- π , and ionic as well as ionic hydrogen bonding to the adsorption of Cl⁻ over functional groups in algal biochar. A comparison of binding energies revealed functional groups at the molecular edge, including those carrying nitrogen such as pyrrole, amide, or amine, as the most favorable sites for Cl⁻ adsorption. Adsorption in these sites was found to be dominated by ionic hydrogen bonding. Depending on the electron density distribution, Cl⁻ could stabilize over the polyaromatic core of algal biochar to form π -bonded complexes, though, with less adsorption energy. This result could be simply caused by the depletion of π electron density of the polyaromatic core owing to the influence of withdrawing substituents that induce less repulsion between anion and π -cloud. Electronic analyses indicated that the nature of functional groups in the molecular structure of biochar influences the electron distribution over the van der Waals surface of biochar and, consequently, impacts the adsorption of the negatively charged chloride ion. Functional groups with electron-withdrawing characteristics like amide, carboxylic, or pyridine attached to the polyaromatic core of biochar were found to increase electron depletion in some parts of the host molecule (biochar) including peripheral hydrogens, causing them more accessible to Cl- adsorption. However, electron accumulation over electron-withdrawing groups gave rise to Cl^- adsorption through a cation-bridging mechanism where the groups paired with Na⁺ ions and turned them into hooks for Cl- ions. The cation-bridging mechanism was found to be associated with higher adsorption energies, significantly improving chloride stabilization on biochar compared with direct adsorption mechanisms. Energy-based data clarify the adsorption strength for Cl⁻ and Na⁺ adsorbate ions and support this hypothesis that electrostatic interactions through direct and indirect adsorption mechanisms increase the capacity of algae biochar to adsorb Cl⁻ and high

stability for the biochar-Cl⁻/Na⁺ complexes. The MD simulations showed the efficacy of nonadecanamide as a representative of N-functional groups in reducing the mobility of chloride.

This study proved that soils amended with algal biochar restrain chloride (and potentially heavy metals), thus helping conserve vegetation, groundwater, and surface water. Algal biochar will also serve as a carbon sequestration tool to decrease CO_2 emissions. Our future research will focus on engineering the biochar chemistry and structure through changing parent feedstocks and the conversion process to produce biochars with enhanced performance in environmental protection.

Author contributions statement

Fulton Schools of **ENGINEERING** School of Sustainable Engineering and the Built Environment Elham (Ellie) H. Fini, Ph.D., P.E. Associate Professor J.W. Fulbright Scholar AAAS-Lemelson Invention Ambassador Arizona State University College Avenue Commons 660 S. College Avenue, Rm 584 Tempe, AZ 85287–3005 Direct: 480-965-4273 E-Mail: efini@asu.edu.

ASU is #1 in the U.S. for Innovation.

Subject: Authors Contribution Statement September 12, 2022.

Dear Editorial Board of the Chemosphere journal,

Please find a copy of our research paper titled "Soil Amended with Algal Biochar Reduces Mobility of Deicing Salt Contaminants in Environment: An Atomistic Insight" for review and possible publication in Chemosphere.

Below please see the statement of contribution from co-authors.

Farideh Pahlavan performed the literature review and conducted molecular modeling and analysis and developed the write-up.

Hamid Ghasemi carried out the literature review, modeling, data analysis, and writing associated with molecular dynamics simulations.

Hessam Yazdani oversaw the molecular dynamics simulations, coprovided funding, and revised the manuscript.

Elham H. Fini provided the research idea and guidance with the research method, conduct of the research, and review of the manuscript.

Thank you very much. Sincerely, Elham H. Fini, Ph. D, P.E.

Declaration of competing interest

The authors declare that they have no known competing financial interests or personal relationships that could have appeared to influence the work reported in this paper.

Data availability

All data used has been shown in the paper

Acknowledgments

This material is based upon work supported by the U.S. National Science Foundation under Grants 2121160 and 2046332. In addition, the authors acknowledge supercomputing centers at the University of Oklahoma and Arizona State University for providing access to HPC resources.

References

Ahmad, M., Rajapaksha, A.U., Lim, J.E., Zhang, M., Bolan, N., Mohan, D., Vithanage, M., Lee, S.S., Ok, Y.S., 2014. Biochar as a sorbent for contaminant management in soil and water: a review. Chemosphere 99, 19–33.

Amonette, J.E., Joseph, S., 2009b. Characteristics of biochar: microchemical properties. In: Lehmann, J., Joseph, S. (Eds.), Biochar for Environmental Management: Science

- and Technology, first ed. Earthscan Publication Ltd., London, UK; Sterling, VA, USA, pp. 33–52.
- Amrhein, C., Strong, J.E., Mosher, P.A., 1992. Effect of deicing salts on metal and organic matter mobilization in roadside soils. Environ. Sci. Technol. 26, 703–709.
- Aruguete, D.M., Wallace, A., Blakney, T., Kerr, R., Gerber, G., Ferko, J., 2020. Palladium release from catalytic converter materials induced by road de-icer components chloride and ferrocyanide. Chemosphere 245, 125578.
- Ashworth, C.R., Matthews, R.P., Welton, T., Hunt, P.A., 2016. Doubly ionic hydrogen bond interactions within the choline chloride–urea deep eutectic solvent. Phys. Chem. Chem. Phys. 18, 18145–18160.
- Awad, Y.M., Blagodatskaya, E., Ok, Y.S., Kuzyakov, Y., 2013. Effects of polyacrylamide, biopolymer and biochar on the decomposition of 14C-labelled maize residues and on their stabilization in soil aggregates. Eur. J. Soil Sci. 64, 488–499.
- Bäckström, M., Karlsson, S., Bäckman, L., Folkeson, L., Lind, B., 2004. Mobilisation of heavy metals by deicing salts in a roadside environment. Water Res. 38, 720–732.
- Burgis, C.R., Hayes, G.M., Henderson, D.A., Zhang, W., Smith, J.A., 2020. Green stormwater infrastructure redirects deicing salt from surface water to groundwater. Sci. Total Environ. 729, 138736.
- Chabi, N., Baghdadi, M., Sani, A.H., Golzary, A., Hosseinzadeh, M., 2020. Removal of tetracycline with aluminum boride carbide and boehmite particles decorated biochar derived from algae. Bioresour. Technol. 316, 123950.
- Chen, W., Chen, Y., Yang, H., Xia, M., Li, K., Chen, X., Chen, H., 2017a. Co-pyrolysis of lignocellulosic biomass and microalgae: products characteristics and interaction effect. Bioresour. Technol. 245, 860–868.
- Chen, Y., Zhang, X., Chen, W., Yang, H., Chen, H., 2017b. The structure evolution of biochar from biomass pyrolysis and its correlation with gas pollutant adsorption performance. Bioresour. Technol. 246, 101–109.
- Chen, H., Tang, L., Hu, Y., Geng, Y., Meng, L., Li, W., Wang, Z., Li, Z., Huo, Z., 2022. Investigating the pathways of enhanced Pb immobilization by chlorine-loaded biochar. J. Clean. Prod. 344, 131097.
- Cheng, C.H., Lehmann, J., Thies, J.E., Burton, S.D., 2008. Stability of black carbon in soils across a climatic gradient. J. Geophys. Res.: Biogeo. 113.
- Clark, T., Hennemann, M., Murray, J.S., Politzer, P., 2007. Halogen bonding: the σ -hole. J. Mol. Model. 13, 291–296.
- Corsi, S.R., De Cicco, L.A., Lutz, M.A., Hirsch, R.M., 2015. River chloride trends in snow-affected urban watersheds: increasing concentrations outpace urban growth rate and are common among all seasons. Sci. Total Environ. 508, 488–497.
- Cubero, E., Luque, F.J., Orozco, M., 1998. Is polarization important in cation-π interactions? Prog. Nat. Sci. 95, 5976–5980.
- Dai, Y., Zhang, N., Xing, C., Cui, Q., Sun, Q., 2019. The adsorption, regeneration and engineering applications of biochar for removal organic pollutants: a review. Chemosphere 223, 12–27.
- Dandamudi, K.P.R., Murdock, T., Lammers, P.J., Deng, S., Fini, E.H., 2021. Production of functionalized carbon from synergistic hydrothermal liquefaction of microalgae and swine manure. Resour. Conserv. Recycl. 170, 105564.
- Deeb, M., Groffman, P.M., Joyner, J.L., Lozefski, G., Paltseva, A., Lin, B., Mania, K., Cao, D.L., McLaughlin, J., Muth, T., 2018. Soil and microbial properties of green infrastructure stormwater management systems. Ecol. Eng. 125, 68–75.
- Delley, B., 1990. An all-electron numerical method for solving the local density functional for polyatomic molecules. J. Chem. Phys. 92, 508–517.
- Delley, B., 2000. From molecules to solids with the DMol 3 approach. J. Chem. Phys. 113, 7756–7764.
- Denich, C., Bradford, A., Drake, J., 2013. Bioretention: assessing effects of winter salt and aggregate application on plant health, media clogging and effluent quality. Water Qual. Res. J. Can. 48, 387–399.
- Downie, A., Crosky, A., Munroe, P., 2009. Physical properties of biochar. In: Lehmann, J., Joseph, S. (Eds.), Biochar for Environmental Management: Science and Technology, 1th ed. Earthscan Publication Ltd., London, UK; Sterling, VA, USA, p. 13e32.
- Equiza, M., Calvo-Polanco, M., Cirelli, D., Señorans, J., Wartenbe, M., Saunders, C., Zwiazek, J., 2017. Long-term impact of road salt (NaCl) on soil and urban trees in Edmonton, Canada. Urban for. Urban Gree 21, 16–28.
- Fan, Q., Sun, J., Chu, L., Cui, L., Quan, G., Yan, J., Hussain, Q., Iqbal, M., 2018. Effects of chemical oxidation on surface oxygen-containing functional groups and adsorption behavior of biochar. Chemosphere 207, 33–40.
- Frisch, M.J.T., , G. W., Schlegel, H.B., Scuseria, G.E., Robb, M.A., Cheeseman, J.R., Scalmani, G., Barone, V., Petersson, G.A., Nakatsuji, H., Li, X., Caricato, M., Marenich, A.V., Bloino, J., Janesko, B.G., Gomperts, R., Mennucci, B., Hratchian, H. P., Ortiz, J.V., Izmaylov, A.F., Sonnenberg, J.L., Williams, Ding, F., Lipparini, F., Egidi, F., Goings, J., Peng, B., Petrone, A., Henderson, T., Ranasinghe, D., Zakrzewski, V.G., Gao, J., Rega, N., Zheng, G., Liang, W., Hada, M., Ehara, M., Toyota, K., Fukuda, R., Hasegawa, J., Ishida, M., Nakajima, T., Honda, Y., Kitao, O., Nakai, H., Vreven, T., Throssell, K., Montgomery Jr., J.A., Peralta, J.E., Ogliaro, F., Bearpark, M.J., Heyd, J.J., Brothers, E.N., Kudin, K.N., Staroverov, V.N., Keith, T.A., Kobayashi, R., Normand, J., Raghavachari, K., Rendell, A.P., Burant, J.C., Iyengar, S. S., Tomasi, J., Cossi, M., Millam, J.M., Klene, M., Adamo, C., Cammi, R., Ochterski, J. W., Martin, R.L., Morokuma, K., Farkas, O., Foresman, J.B., Fox, D.J., 2016. Gaussian 16 Rev. C.01. Wallingford, CT.
- Ghasemi, H., Hatam-Lee, S.M., Tirkolaei, H.K., Yazdani, H., 2022a. Biocementation of soils of different surface chemistries via enzyme induced carbonate precipitation (EICP): an integrated laboratory and molecular dynamics study. Biophys. Chem. 284, 106793.
- Ghasemi, H., Yazdani, H., Rajib, A., Fini, E.H., 2022b. Toward carbon-negative and emission-curbing roads to drive environmental health. ACS Sustain. Chem. Eng. 10, 1857–1862.

- Giese, M., Albrecht, M., Bannwarth, C., Raabe, G., Valkonen, A., Rissanen, K., 2011. From attraction to repulsion: anion–π interactions between bromide and fluorinated phenyl groups. Chem. Commun. 47, 8542–8544.
- Giese, M., Albrecht, M., Rissanen, K., 2016. Experimental investigation of anion–π interactions–applications and biochemical relevance. Chem. Commun. 52, 1778–1795.
- Glaser, B., Lehmann, J., Zech, W., 2002. Ameliorating physical and chemical properties of highly weathered soils in the tropics with charcoal–a review. Biol. Fertil. Soils 35, 219–230.
- Grimme, S., 2011. Density functional theory with London dispersion corrections. WIRES. Comput. Mol. Sci. 1, 211–228.
- Hajikarimi, P., Onochie, A., Fini, E.H., 2020. Characterizing mechanical response of biomodified bitumen at sub zero temperatures. Construct. Build. Mater. 240, 117940.
- Hennemann, M., Murray, J.S., Politzer, P., Riley, K.E., Clark, T., 2012. Polarization-induced σ -holes and hydrogen bonding. J. Mol. Model. 18, 2461–2469.
- Hintz, W.D., Mattes, B.M., Schuler, M.S., Jones, D.K., Stoler, A.B., Lind, L., Relyea, R.A., 2017. Salinization triggers a trophic cascade in experimental freshwater communities with varying food-chain length. Ecol. Appl. 27, 833–844.
- Hintz, W.D., Fay, L., Relyea, R.A., 2022. Road salts, human safety, and the rising salinity of our fresh waters. Front. Ecol. Environ. 20, 22–30.
- Howard, K.W., Haynes, J., 1993. Groundwater Contamination Due to Road De-icing Chemicals—Salt Balance Implications. Geoscience Canada.
- Huang, Y., Tian, Z., Ke, Q., Liu, J., Irannezhad, M., Fan, D., Hou, M., Sun, L., 2020. Nature-based solutions for urban pluvial flood risk management. WIREs Water 7, e1421
- Humphrey, W., Dalke, A., Schulten, K., 1996. VMD: visual molecular dynamics. J. Mol. Graph. 14, 33–38.
- Hunter, C.A., 2004. Quantifying intermolecular interactions: guidelines for the molecular recognition toolbox. Angew. Chem., Int. Ed. 43, 5310–5324.
- Inyang, M., Dickenson, E., 2015. The potential role of biochar in the removal of organic and microbial contaminants from potable and reuse water: a review. Chemosphere 134, 232–240.
- Jia, Y., Xiao, B., Thomas, K., 2002. Adsorption of metal ions on nitrogen surface functional groups in activated carbons. Langmuir 18, 470–478.
- Jiang, Z., Lian, F., Wang, Z., Xing, B., 2020. The role of biochars in sustainable crop production and soil resiliency. J. Exp. Bot. 71, 520–542.
- Jones, D.K., Mattes, B.M., Hintz, W.D., Schuler, M.S., Stoler, A.B., Lind, L.A., Cooper, R. O., Relyea, R.A., 2017. Investigation of road salts and biotic stressors on freshwater wetland communities. Environ. Pollut. 221, 159–167.
- Kaushal, S.S., Likens, G.E., Pace, M.L., Utz, R.M., Haq, S., Gorman, J., Grese, M., 2018. Freshwater salinization syndrome on a continental scale. P. Natl. A. Sci. 115, E574–E583.
- Keeley, M., Koburger, A., Dolowitz, D.P., Medearis, D., Nickel, D., Shuster, W., 2013. Perspectives on the use of green infrastructure for stormwater management in Cleveland and Milwaukee. Environ. Manag. 51, 1093–1108.
- Keiluweit, M., Nico, P.S., Johnson, M.G., Kleber, M., 2010. Dynamic molecular structure of plant biomass-derived black carbon (biochar). Environ. Sci. Technol. 44, 1247–1253.
- Kuzyakov, Y., Subbotina, I., Chen, H., Bogomolova, I., Xu, X., 2009. Soil Biol. Biochem. 41, 210–219.
- Lefebvre, C., Rubez, G., Khartabil, H., Boisson, J.-C., Contreras-García, J., Henon, E., 2017. Accurately extracting the signature of intermolecular interactions present in the NCI plot of the reduced density gradient versus electron density. Phys. Chem. Chem. Phys. 19, 17928–17936.
- Lefebvre, C., Khartabil, H., Boisson, J.C., Contreras-García, J., Piquemal, J.P., Hénon, E., 2018. The independent gradient model: a new approach for probing strong and weak interactions in molecules from wave function calculations. ChemPhysChem 19, 724–735
- Lehmann, J., Joseph, S., 2009. Biochar for environmental management: an introduction. In: Lehmann, J., Joseph, S. (Eds.), Biochar for Environmental Management Science and Technology, pp. 1–12. Earthscans, UK.
- Lehmann, J., Skjemstad, J., Sohi, S., Carter, J., Barson, M., Falloon, P., Coleman, K., Woodbury, P., Krull, E., 2008. Australian climate–carbon cycle feedback reduced by soil black carbon. Nat. Geosci. 1, 832–835.
- Leng, L.-j., Yuan, X.-z., Huang, H.-j., Wang, H., Wu, Z.-b., Fu, L.-h., Peng, X., Chen, X.-h., Zeng, G.-m., 2015. Characterization and application of bio-chars from liquefaction of microalgae, lignocellulosic biomass and sewage sludge. Fuel Process. Technol. 129, 8–14.
- Leng, L., Xu, S., Liu, R., Yu, T., Zhuo, X., Leng, S., Xiong, Q., Huang, H., 2020. Nitrogen containing functional groups of biochar: an overview. Bioresour. Technol. 298, 122286.
- Li, S., Harris, S., Anandhi, A., Chen, G., 2019. Predicting biochar properties and functions based on feedstock and pyrolysis temperature: a review and data syntheses. J. Clean. Prod. 215, 890–902.
- Lohrasebi, A., Rikhtehgaran, S., 2018. Ion separation and water purification by applying external electric field on porous graphene membrane. Nano Res. 11, 2229–2236.
- Lu, T., Chen, F., 2012. Multiwfn: a multifunctional wavefunction analyzer. J. Comput. Chem. 33, 580–592.
- Lu, T., Chen, Q., 2021. Independent Gradient Model Based on Hirshfeld Partition (IGMH): A New Method for Visual Study of Interactions in Chemical Systems.
- Lu, T., Chen, Q., 2022. Independent gradient model based on Hirshfeld partition: a new method for visual study of interactions in chemical systems. J. Comput. Chem. 43, 539–555.
- Maliutina, K., Tahmasebi, A., Yu, J., Saltykov, S.N., 2017. Comparative study on flash pyrolysis characteristics of microalgal and lignocellulosic biomass in entrained-flow reactor. Energy Convers. Manag. 151, 426–438.

Maliutina, K., Tahmasebi, A., Yu, J., 2018a. Pressurized entrained-flow pyrolysis of microalgae: enhanced production of hydrogen and nitrogen-containing compounds. Bioresour. Technol. 256, 160–169.

- Maliutina, K., Tahmasebi, A., Yu, J., 2018b. The transformation of nitrogen during pressurized entrained-flow pyrolysis of Chlorella vulgaris. Bioresour. Technol. 262, 90–97
- Marsalek, J., 2003. Road salts in urban stormwater: an emerging issue in stormwater management in cold climates. Water Sci. Technol. 48, 61–70.
- McFarland, A.R., Larsen, L., Yeshitela, K., Engida, A.N., Love, N.G., 2019. Guide for using green infrastructure in urban environments for stormwater management. Environ. Sci.-Wat. Res. 5, 643–659.
- Meot-Ner, M., 2012. Update 1 of: strong ionic hydrogen bonds. Chem. Rev. 112, PR22–PR103.
- Mohan, D., Sarswat, A., Ok, Y.S., Pittman Jr., C.U., 2014. Organic and inorganic contaminants removal from water with biochar, a renewable, low cost and sustainable adsorbent–a critical review. Bioresour. Technol. 160, 191–202.
- Mousavi, M., Martis, V., Fini, E.H., 2021. Inherently functionalized carbon from algae to adsorb precursors of secondary organic aerosols in noncombustion sources. ACS Sustain. Chem. Eng. 9, 14375–14384.
- Mukherjee, A., Zimmerman, A., Harris, W., 2011. Surface chemistry variations among a series of laboratory-produced biochars. Geoderma 163, 247–255.
- Mullins, A.R., Bain, D.J., Pfeil-McCullough, E., Hopkins, K.G., Lavin, S., Copeland, E., 2020. Seasonal drivers of chemical and hydrological patterns in roadside infiltrationbased green infrastructure. Sci. Total Environ. 714, 136503.
- Olmo, M., Villar, R., Salazar, P., Alburquerque, J.A., 2016. Changes in soil nutrient availability explain biochar's impact on wheat root development. Plant Soil 399, 333–343.
- Panahi, H.K.S., Dehhaghi, M., Ok, Y.S., Nizami, A.-S., Khoshnevisan, B., Mussatto, S.I., Aghbashlo, M., Tabatabaei, M., Lam, S.S., 2020. A comprehensive review of engineered biochar: production, characteristics, and environmental applications. J. Clean. Prod. 270, 122462.
- Pandey, B., Suthar, S., Chand, N., 2022. Effect of biochar amendment on metal mobility, phytotoxicity, soil enzymes, and metal-uptakes by wheat (Triticum aestivum) in contaminated soils. Chemosphere, 135889.
- Partenio, A., 2020. Retrofitting Resilience in Red Hook, Brooklyn: A Roadmap for Neighborhood-Scale Integration of Green Infrastructure. Columbia University.
- Paus, K.H., Morgan, J., Gulliver, J.S., Hozalski, R.M., 2014. Effects of bioretention media compost volume fraction on toxic metals removal, hydraulic conductivity, and phosphorous release. J. Environ. Eng. 140, 04014033.
- Perdew, J.P., Burke, K., Ernzerhof, M., 1996. Generalized gradient approximation made simple. Phys. Rev. Lett. 77, 3865.
- Politzer, P., Murray, J.S., Peralta-Inga, Z., 2001. Molecular surface electrostatic potentials in relation to noncovalent interactions in biological systems. Int. J. Quant. Chem. 85, 676–684.
- Politzer, P., Murray, J.S., Clark, T., 2010. Halogen bonding: an electrostatically-driven highly directional noncovalent interaction. Phys. Chem. Chem. Phys. 12, 7748–7757.
- Purakayastha, T., Kumari, S., Pathak, H., 2015. Characterisation, stability, and microbial effects of four biochars produced from crop residues. Geoderma 239, 293–303.
- Qiu, Y., Ichiba, A., Paz, I.D.S.R., Chen, F., Versini, P.-A., Schertzer, D., Tchiguirinskaia, I., 2019. Evaluation of low impact development and nature-based solutions for stormwater management: a fully distributed modelling approach. Hydrol. Earth Syst. Sci. Discuss. 1–27
- Quiñonero, D., Garau, C., Frontera, A., Ballester, P., Costa, A., Deyà, P.M., 2002. Counterintuitive interaction of anions with benzene derivatives. Chem. Phys. Lett. 359, 486–492.
- Quiñonero, D., Garau, C., Rotger, C., Frontera, A., Ballester, P., Costa, A., Deyà, P.M., 2004. Anion– π interactions: do they exist? Angew. Chem- Ger. Edit 116, 142-142.
- Rajib, A., Fini, E.H., 2020. Inherently functionalized carbon from lipid and protein-rich biomass to reduce ultraviolet-induced damages in bituminous materials. ACS Omega 5. 25273–25280.
- Rajib, A., Saadeh, S., Katawal, P., Mobasher, B., Fini, E.H., 2021. Enhancing biomass value chain by utilizing biochar as A free radical scavenger to delay ultraviolet aging of bituminous composites used in outdoor construction. Resour. Conserv. Recycl. 168, 105302.

Robinson, H.K., Hasenmueller, E.A., Chambers, L.G., 2017. Soil as a reservoir for road salt retention leading to its gradual release to groundwater. Appl. Geochem. 83, 72–85

- Saadeh, S., Al-Zubi, Y., Katawal, P., Zaatarah, B., Fini, E., 2021. Biochar Effects on the Performance of Conventional and Rubberized HMA. Road Mater. Pavement, pp. 1–17.
- Sajjadi, B., Zubatiuk, T., Leszczynska, D., Leszczynski, J., Chen, W.Y., 2019. Chemical activation of biochar for energy and environmental applications: a comprehensive review. Rev. Chem. Eng. 35, 777–815.
- Sánchez-García, M., Cayuela, M.L., Rasse, D.P., Sánchez-Monedero, M.A., 2019. Biochars from mediterranean agroindustry residues: physicochemical properties relevant for C sequestration and soil water retention. ACS Sustain. Chem. Eng. 7, 4724–4733.
- Schottel, B.L., Chifotides, H.T., Dunbar, K.R., 2008. Anion- π interactions. Chem. Soc. Rev. 37, 68–83.
- Schuler, M.S., Relyea, R.A., 2018. A review of the combined threats of road salts and heavy metals to freshwater systems. Bioscience 68, 327–335.
- Semadeni-Davies, A., 2006. Winter performance of an urban stormwater pond in southern Sweden. Hydrol. Process- Int. J. 20, 165–182.
- Shackley, S., Carter, S., Knowles, T., Middelink, E., Haefele, S., Sohi, S., Cross, A., Haszeldine, S., 2012. Sustainable gasification–biochar systems? A case-study of ricehusk gasification in Cambodia, Part I: context, chemical properties, environmental and health and safety issues. Energy Pol. 42, 49–58.
- Singh, B.P., Cowie, A.L., Smernik, R.J., 2012. Biochar carbon stability in a clayey soil as a function of feedstock and pyrolysis temperature. Environ. Sci. Technol. 46, 11770–11778.
- Snodgrass, J.W., Moore, J., Lev, S.M., Casey, R.E., Ownby, D.R., Flora, R.F., Izzo, G., 2017. Influence of modern stormwater management practices on transport of road salt to surface waters. Environ. Sci. Technol. 51, 4165–4172.
- Sohi, S., Lopez-Capel, E., Krull, E., Bol, R., 2009. Biochar's Roles in Soil and Climate Change: A Review of Research Needs, vol. 5. CSIRO Land and Water Science Report, pp. 1–57.
- Stagge, J.H., Davis, A.P., Jamil, E., Kim, H., 2012. Performance of grass swales for improving water quality from highway runoff. Water Res. 46, 6731–6742.
- Sun, Z., Chai, L., Shu, Y., Li, Q., Liu, M., Qiu, D., 2017. Chemical bond between chloride ions and surface carboxyl groups on activated carbon. Colloid. Surface. 530, 53–59.
- Thompson, A.P., Aktulga, H.M., Berger, R., Bolintineanu, D.S., Brown, W.M., Crozier, P. S., Veld, P.J., Kohlmeyer, A., Moore, S.G., Nguyen, T.D., 2022. LAMMPS-a flexible simulation tool for particle-based materials modeling at the atomic, meso, and continuum scales. Comput. Phys. Commun. 271, 108171 in't.
- Van Duin, A.C., Dasgupta, S., Lorant, F., Goddard, W.A., 2001. ReaxFF: a reactive force field for hydrocarbons. J. Phys. Chem. A 105, 9396–9409.
- Verheijen, F., Jeffery, S., Bastos, A.C., van der Velde, M., Diafas, I., 2010. Biochar Application to Soils. A Critical Scientific Review of Effects on Soil Properties, Processes and Functions. European Commission, Italy.
- Wang, T., Wu, J., Zhang, Y., Liu, J., Sui, Z., Zhang, H., Chen, W.-Y., Norris, P., Pan, W.-P., 2018. Increasing the chlorine active sites in the micropores of biochar for improved mercury adsorption. Fuel 229, 60–67.
- Wheeler, S.E., Bloom, J.W., 2014. Toward a more complete understanding of noncovalent interactions involving aromatic rings. J. Phys. Chem. A 118, 6133–6147.
- Xi, J., Zhou, Z., Yuan, Y., Xiao, K., Qin, Y., Wang, K., An, Y., Ye, J., Wu, Z., 2022. Enhanced nutrient removal from stormwater runoff by a compact on-site treatment system. Chemosphere 290, 133314.
- Zhang, X., Zhang, S., Yang, H., Shao, J., Chen, Y., Liao, X., Wang, X., Chen, H., 2017. Generalized two-dimensional correlation infrared spectroscopy to reveal mechanisms of CO2 capture in nitrogen enriched biochar. Proc. Combust. Inst. 36, 3933–3940.
- Zhou, T., Kabir, S.F., Cao, L., Luan, H., Dong, Z., Fini, E.H., 2020. Comparing effects of physisorption and chemisorption of bio-oil onto rubber particles in asphalt. J. Clean. Prod. 273, 123112.
- Zhu, D., Pignatello, J.J., 2005. Characterization of aromatic compound sorptive interactions with black carbon (charcoal) assisted by graphite as a model. Environ. Sci. Technol. 39, 2033–2041.